Complex dynamics of current filaments in the low-temperature impurity breakdown regime of semiconductors

G. Hüpper, K. Pyragas,* and E. Schöll
Institut für Theoretische Physik, Technische Universität Berlin, Hardenbergstrasse 36, D-1000 Berlin 12, Germany
(Received 1 December 1992)

The formation of spatial and spatiotemporal patterns (current filaments) in semiconductors in the regime of low-temperature impurity impact ionization is investigated theoretically. Our model yields stable filaments, breathing filaments, and traveling filaments which show an intermittent spatiotemporal instability, resulting in chaotic oscillations of the average carrier density and of the current. The crucial role of the dielectric relaxation of the transverse electric field is singled out. Different strategies for the numerical treatment are discussed.

I. INTRODUCTION

Current filaments in semiconductors are self-organized spatial structures which are associated with a transversally modulated inhomogeneous current flow. Such current filaments have been observed in the low-temperature impurity breakdown of n-type GaAs (Refs. 1–3) and p-type Ge,[4] as well as at room temperature in Si p-i-n diodes[5] and p-n-p-n diodes.[6,7] The filaments are usually connected with an S-shaped current-voltage characteristic with negative differential conductivity (SNDC).

In this paper, we theoretically investigate the formation and evolution of current filaments in the low-temperature regime. Our model is based upon coupled nonlinear partial differential equations with only one diffusive variable, viz., the carrier density, and includes the dynamics of the electric field. Previous models proposed for this physical system deal with stationary spatial structures,[8] linear modes of the current filaments,[9] or homogeneous oscillations.[10–12] Other descriptions parametrize the dynamics of the spatial inhomogeneity with few order parameters.[13,14] Our model will extend these studies to describe the full nonlinear spatiotemporal dynamics of the filaments. As a result, we are able to explain in detail the complex, turbulent dynamics occurring far from thermodynamic equilibrium.

II. THE MODEL

As the relevant dynamic variables for the description of the charge transport in the semiconductor, we choose the density of the free majority carriers n and of the carriers bound at M shallow impurity levels n_i $(i=1,\ldots,M)$ corresponding to ground and excited states. These are coupled to the electric field $\mathcal{E}$ via Maxwell's equations. In this analysis, we make the following assumptions.[15]

(1) Momentum relaxation occurs faster than all other processes, so that the mean momentum per carrier $\mathbf{p}$ can be eliminated adiabatically.

(2) The mean energy E of the carriers is also a fast variable with a small heat diffusion constant. This implies a local energy-field relation

$$E=E_0+\frac{\eta}{2}m^*\mu^2\mathcal{E}^2\ , \tag{1}$$

where $E_0=(\frac{3}{2})k_BT_L$ is the thermal equilibrium energy, m^* is the effective mass, μ is the mobility of the carriers, $\eta=2\tau_e/\tau_m$ is twice the ratio of the energy and momentum relaxation times, k_B is the Boltzmann constant, and T_L is the lattice temperature.

(3) As shown experimentally[4,16–18] and theoretically,[19] the dominant structure formation in the system considered occurs perpendicular to the current flow, in the form of current filaments. Thus we assume spatial inhomogeneity only in this direction. Experimentally, spatial structures in the direction parallel to the current flow, e.g., mainly a distortion of the filament walls due to contact effects, have also been observed. However, for sufficiently large contact spacing, the essential spatial structure is in the transverse direction.

(4) Since all occurring velocities are much smaller than the velocity of light in the semiconductor material, the electric field is treated as purely longitudinal, i.e., free of vortices ($\nabla\times\mathcal{E}=0$).

Let us choose the coordinate system such that the drift current and the drift field ($\mathcal{E}_x$) are in the x direction, and the internal space-charge field $\mathcal{E}_z$ due to current filamentation is in the z direction. The sample is considered to be sufficiently small in the y direction so that we can assume homogeneity in this direction (this allows for *plane filaments*). From a moment expansion of the Boltzmann equation, we obtain the balance equations[20–22]

$$\frac{\partial n}{\partial t}+\frac{\partial(nv_z)}{\partial z}=\phi(n,\vec{n}_t,\mathcal{E})\ , \tag{2}$$

$$\frac{\partial\vec{n}_t}{\partial t}=\vec{\phi}_t(n,\vec{n}_t,\mathcal{E})\ , \tag{3}$$

with mean transverse velocity $v_z=\mu[\mathcal{E}_z-(1/n)\partial n/\partial z]$ and generation-recombination (GR) rates ϕ and $\vec{\phi}_t$, with $\phi+\sum_{i=1}^{M}\phi_i=0$. Here we have introduced M-dimensional vector fields $\vec{n}_t=(n_1,\ldots,n_M)$ and $\vec{\phi}_t=(\phi_1,\ldots,\phi_M)$. Note that all quantities are given in dimensionless units

TABLE I. Dimensionless variables.

Quantity	Unit
μ	μ_0 (low-field mobility)
$n,\vec{n}_t$	$N_A^*=N_A-N_D$
t	$\tau_M^*=\dfrac{\varepsilon}{e\mu_0 N_A^*}$
z	$L_D=\left[\dfrac{k_B T_L \varepsilon}{e^2 N_A^*}\right]^{1/2}$
$\mathcal{E}$	$\mathcal{E}_0=\dfrac{k_B T_L}{eL_D}$

as listed in Table I. We have assumed p-type material where the carriers are holes, but the results can be easily transferred to n type. Since the electric field is free of vortices, $\mathcal{E}_x$ cannot depend on the spatial coordinate: $\partial\mathcal{E}_x/\partial z=0$. Additionally, the local charge density ρ couples with the electric field via Poisson's equation

$$\frac{\partial\mathcal{E}_z}{\partial z}=\rho=n+\sum_{i=1}^{M} n_i-1 \ . \tag{4}$$

The sample is connected to a constant voltage source U_0 via a load resistor R in series and a parallel capacitor C. The time evolution of the electric field due to dielectric relaxation is given by

$$c_r\frac{\partial\mathcal{E}_x}{\partial t}=j_0-(\mu\langle n\rangle+\sigma_L)\mathcal{E}_x \ , \tag{5}$$

$$\frac{\partial\mathcal{E}_z}{\partial t}=-\mu\left[n\mathcal{E}_z-\frac{\partial n}{\partial z}\right] , \tag{6}$$

where $c_r=1+LC/(A\varepsilon)$, A is the cross section of the sample, L is the size of the sample in the x direction, $j_0=U_0/(RAe\mu_0 N_A^*\mathcal{E}_0)$, $\sigma_L=L/(RAe\mu_0 N_A^*)$, $\varepsilon=\varepsilon_r\varepsilon_0$ is the relative and absolute permittivity. For the current balance (5) we have integrated the total current density $\mathbf{j}^{\rm tot}=\partial\mathcal{E}/\partial t+\mathbf{j}$ over the cross section of the sample, taking into account $\mathrm{div}\mathbf{j}^{\rm tot}=0$. The brackets denote the spatial average over the sample width W: $\langle n\rangle\equiv\int_0^W n\,dz/W$.

Equation (6) can be obtained by adding (2) and (3) and combining the result with Eq. (4).

III. THE HOMOGENEOUS STEADY STATES

The spatially homogeneous steady states (denoted by $*$) are obtained by setting all temporal and spatial derivatives in (2)–(6) equal to zero. For common GR kinetics, the GR rates are linear in $\vec{n}_t$,[19] so (3) leads to a unique relation between $\vec{n}_t$ and $n,\mathcal{E}$ of the form $\vec{n}_t^*(n,\mathcal{E})$. This implies that the steady-state charge density can be expressed as a function of $n,\mathcal{E}$ alone: $\rho^*(n,\mathcal{E})$. Further, $\mathcal{E}_z^*=0$ holds by (6). The steady states are given by the condition of local charge neutrality [$\rho^*(n,\mathcal{E})=0$ by (4)] and by the static current-density-field relation $j_0(n,\mathcal{E})$ [by (5)]. Bistability of the homogeneous steady state can occur if $\rho^*(n,\mathcal{E})=0$ has more than one solution $n^*(\mathcal{E})$ in a certain field range. This can be achieved if more than one impurity level is taken into account.[19]

As an explicit example, we refer to p-type Ge at 4 K. We consider two impurity levels (the ground level n_1 and the first excited level n_2). The GR kinetics is given by[19]

$$\phi=X_1^s n_2-T_1^s n(N_A/N_A^*-n_1-n_2)+X_1 n n_1+X_1^* n n_2 \ , \tag{7}$$

$$\phi_1=T^* n_2-X^* n_1-X_1 n n_1 \ , \tag{8}$$

$$\phi_2=-\phi-\phi_1 \ , \tag{9}$$

where X_1^s is the thermal ionization coefficient of the excited level, T_1^s is its hole capture coefficient, X_1 and X_1^* are the hole impact ionization coefficients from the ground and excited levels, respectively, X^* and T^* denote the transition coefficients from the ground to the excited level, and vice versa, respectively.

In the following, the GR coefficients as a function of the electric field $\mathcal{E}=(\mathcal{E}_x^2+\mathcal{E}_z^2)^{1/2}$ are obtained by a spatially homogeneous Monte Carlo (MC) simulation.[23] The numerical parameters used for the GR processes, X^*, T^*, and X_1^s (see Table II), have been calculated on the basis of the Lax cascade-capture model,[24–26] using de-

TABLE II. Material parameters for p-type Ge at 4 K.

$N_A=10^{14}$ cm^{-3}, $N_D=5\times10^{12}$ cm^{-3}, $\varepsilon_r=16$, $T_L=4$ K, $\mu=\mu_0=10^5$ cm^2/V s
$\tau_M^*=10^{-12}$ s, $L_D=5.6\times10^{-6}$ cm, $\mathcal{E}_0=60.8$ V/cm
$X^*=10^{-15}$, $T^*=7.21\times10^{-5}$, $X_1^s=1.4\times10^{-6}$
$X_1(\mathcal{E})=x_1\exp[-x_2(\alpha\mathcal{E})^{x_3}]$
$X_1^*(\mathcal{E})=x_1^*\exp[-x_2^*(\alpha\mathcal{E})^{x_3^*}]$
$T_1^s(\mathcal{E})=t_1\exp[-t_2(t_3+\alpha\mathcal{E})^2]+t_4(t_5+\alpha\mathcal{E})^{t_6}$

with

$x_1=7.85\times10^{-4}$	$x_1^*=4.18\times10^{-2}$	$t_1=-1.2\times10^{-3}$
$x_2=11.3$	$x_2^*=3.72$	$t_2=0.2$
$x_3=-0.745$	$x_3^*=-0.66$	$t_3=-0.254$
$\alpha=60.8$		$t_4=1.73\times10^{-3}$
		$t_5=0.421$
		$t_6=-0.887$

tailed balance.[19] The MC transport data are fitted by smooth functions of the electric field yielding SNDC in the resulting carrier density-field characteristic (Fig. 1). This multistationarity can be explained in the following manner: for low electric fields, almost all carriers are trapped in the ground state of the impurities. When the electric field increases, the few carriers in the valence band gain energy in the field, until they are able to impact ionize carriers from the ground level (note that the excited level is not populated). The breakdown occurs in the field regime that corresponds to the (higher) energy needed to ionize carriers from the ground level. When the electric field decreases, the carriers in the band will be trapped in the excited level. Since the transition time to the ground state is very long, the population of the excited level will be high until the energy of the free carriers is too small to ionize the carriers in the excited level. So the freeze-out occurs in the field regime corresponding to the (lower) energy needed to ionize carriers from the excited level. This results in a hysteresis under voltage control.

IV. STABILITY OF THE HOMOGENEOUS STEADY STATES

The stability of the homogeneous steady states of the system $\Phi^*=(n^*,\vec{n}_t^*,\mathcal{E}_x^*,\mathcal{E}_z^*)$ against small fluctuations $\delta\Phi(z,t)=\delta\Phi_0 e^{ikz}e^{\lambda t}$ can be determined by linearizing (2)–(6) around this steady state. Most of this linear stability analysis has been reported previously,[19] so here we give only a brief summary.

Since the electric field is vortex free, $k\delta\mathcal{E}_x=0$ holds. This implies that only homogeneous modes ($k=0$) allow for $\delta\mathcal{E}_x\neq 0$. This motivates the separate treatment of homogeneous and inhomogeneous modes.

In the rest of this paper, we restrict ourselves to the case of $c_r=1$ (no external capacitance) and $\sigma_L=0$ (current source).

For the case $k\neq 0$, $\delta\mathcal{E}_x=0$ holds, so that the linearized Eq. (5) can be neglected. In this case, a Fourier transformation of the linearized system leads to $M+1$ branches of the dispersion relation $\lambda(k)$, since the dynamics of the $M+3$ dynamic variables $n,\vec{n}_t,\mathcal{E}_x,\mathcal{E}_z$ is restricted through $\delta\mathcal{E}_x=0$ and the Poisson equation (4).

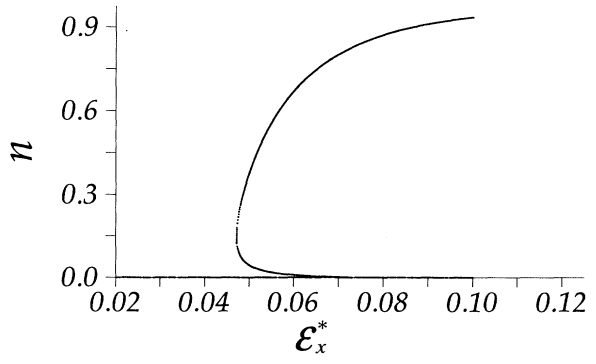

FIG. 1. The homogeneous steady-state carrier density n in units of N_A^* vs the steady-state longitudinal electric field in units of $\mathcal{E}_0$ calculated with the parameters of Table II.

Since for normal GR kinetics, the rates are linear in $\vec{n}_t$, (3) leads to

$$\lambda\delta\vec{n}_t=B(n)\delta\vec{n}_t+\vec{d}\delta n\ , \tag{10}$$

where the components of the matrix B and the vector $\vec{d}$ are given by $B_{ij}=\partial\phi_i/\partial n_j$ and $d_i=\partial\phi_i/\partial n$. Thus the fluctuations $\delta\vec{n}_t$ can be expressed by δn only:

$$\delta\vec{n}_t=\frac{-\mathrm{adj}(B-\lambda)}{G(\lambda)}\vec{d}\delta n\ , \tag{11}$$

where $G(\lambda)=\det(B-\lambda)$, and $(\mathrm{adj}B)_{i,j}$ is $(-1)^{1+j}$ times the determinant of the matrix obtained by deleting the jth row and the ith column of B (adjunct of B). The zeros of $G(\lambda)$ describe fluctuations of the trapped hole concentrations, with $\delta n=0$ and $\delta\mathcal{E}_z=0$. Linearizing and differentiating (6) with respect to z can be combined with (4) to the eigenmode equation

$$V(\lambda)\equiv(\lambda+\mu n^*)\frac{H(\lambda)}{G(\lambda)}=-\mu k^2\ , \tag{12}$$

where $H(\lambda)=G(\lambda)-\sum_{i,j}\mathrm{adj}(B-\lambda)_{ij}d_j=\det(A_{\mathrm{GR}}-\lambda)$. A_{GR} is the Jacobian matrix of the subsystem describing the charge-neutral fluctuations of the carrier densities with $\delta\mathcal{E}=0$ and $\delta\rho=0$.

The time scales introduced in the model are (i) the time associated with the transport of the carriers, i.e., the dielectric relaxation time τ_M^*, and (ii) the GR lifetime τ_{GR}. Depending on the ratios of these time scales, three major regimes can be identified: (a) $\tau_M^*\gg\tau_{\mathrm{GR}}$ (relaxation semiconductor, corresponding to low conductivity); (b) $\tau_M^*\ll\tau_{\mathrm{GR}}$ (lifetime semiconductor, corresponding to high conductivity); and (c) $\tau_M^*\approx\tau_{\mathrm{GR}}$ (intermediate regime).

For *lifetime* semiconductors, we can drop the left-hand side of (6) and obtain

$$n^*\frac{H(\lambda)}{G(\lambda)}=-k^2\ . \tag{13}$$

For *relaxation* semiconductors, we can drop the left-hand side of (3), thus

$$\delta\rho=\frac{H(0)}{G(0)}\delta n\ , \tag{14}$$

where $H(0)=\det A_{\mathrm{GR}}$ and $G(0)=\det B$. This adiabatic elimination of the fast carrier dynamics is only valid if the obtained quasistationary state is stable against fluctuations of the fast variables.[27] We obtain the linearized continuity equation by summing up (3) and (2):

$$\lambda\delta\rho=-\mu\left[n^*+k^2\frac{G(0)}{H(0)}\right]\delta\rho\ . \tag{15}$$

In conclusion, we obtain the eigenvalue equations by (14), (15), and (6):

$$\lambda\delta\rho=-\mu\left[n^*+k^2\frac{G(0)}{H(0)}\right]\delta\rho\ , \tag{16}$$

$$\lambda\delta\mathcal{E}_z=-\mu\left[n^*\delta\mathcal{E}_z-ik\frac{G(0)}{H(0)}\delta\rho\right]\ , \tag{17}$$

with the eigenvalues

$$\lambda_1=-\mu n^* \ , \quad \lambda_2=-\mu\left[n^*+k^2\frac{G(0)}{H(0)}\right] . \tag{18}$$

The last term can be connected with the stationary homogeneous current-density-field relation. Since, under steady-state conditions,

$$\vec{\phi}_t(n,\vec{n}_t^*(n,\mathcal{E}_z),\mathcal{E}_z)=0 \tag{19}$$

holds, the total derivative of $\vec{\phi}_t$ with respect to X (where X is n or $\mathcal{E}_z$) vanishes:

$$\frac{d\vec{\phi}_t}{dX}=\frac{\partial\vec{\phi}_t}{\partial X}+B\frac{d\vec{n}_t}{dX}=0 \ , \tag{20}$$

thus

$$\frac{d\vec{n}_t}{dX}=-B^{-1}\frac{\partial\vec{\phi}_t}{\partial X} . \tag{21}$$

With $X=n$, we obtain

$$\left[\frac{\partial\rho}{\partial n}\right]_{\mathcal{E}}=\frac{H(0)}{G(0)} . \tag{22}$$

With this, the eigenvalues (18) read

$$\lambda_1=-\mu n^* \ , \quad \lambda_2=-\mu\left[n^*+k^2\left[\frac{\partial\rho}{\partial n}\right]_{\mathcal{E}}^{-1}\right] , \tag{23}$$

where λ_1 corresponds to a pure damped dielectric relaxation mode and λ_2 to a coupled-relaxation–GR mode, which may be unstable on the NDC branch of the current-voltage characteristic because $(\partial\rho/\partial n)_{\mathcal{E}}<0$ holds there.

Equation (22) implies an important general theorem about the stability of the homogeneous steady states,[19]

$$\prod_{i=1}^{M+1}\lambda_i(0)=H(0)=G(0)\left[\frac{\partial\rho}{\partial n}\right]_{\mathcal{E}} . \tag{24}$$

The eigenvalues associated with $G(\lambda)$ are usually all negative [which can be proven for the specific GR rates in (8) and (9)]. Since ρ is a continuous function of n, the right-hand side of (24) changes sign between consecutive zeros. This implies that stable and unstable steady states alternate for fixed electric field.

Figure 2 shows the resulting dispersion relations for the special model (7)–(9). For the higher current density [Fig. 2(a)], the eigenvalue spectrum according to (12) matches perfectly with that from (13) which allows us to neglect the fast transversal dielectric relaxation in this regime. For the lower current density [Figs. 2(b) and 2(c)], significant differences are seen between the full solution (continuous line) and the lifetime approximation (dashed), thus the full system has to be investigated. We note that the current density j_0 for both Figs. 2(a) and 2(b) corresponds to steady states on the NDC branch of the characteristic in Fig. 1. In both cases, an instability $\mathrm{Re}\lambda>0$ occurs for a range of k vectors.

For homogeneous modes ($k=0$), a necessary condition for an oscillatory instability (Hopf bifurcation) of the special model (8) and (9) is $ndv/d\mathcal{E}<\lambda_1$, where λ_1 is the largest eigenvalue of A_{GR}.[19] This condition can only be achieved on the NDC branch of the static current-field characteristic if the concentration n is low and the differential mobility $dv/d\mathcal{E}$ is small and positive. It turns out that for our material parameters the system is stable against homogeneous fluctuations.

As a result, we obtain a long-wavelength instability on the NDC branch. Fluctuations with a wave vector $k<k_c$ grow in time, where k_c is the marginal wave vector with $\lambda(k_c)=0$. These inhomogeneous fluctuations trigger the formation of current filaments. The physical origin of this instability is the autocatalytic impact ionization process.

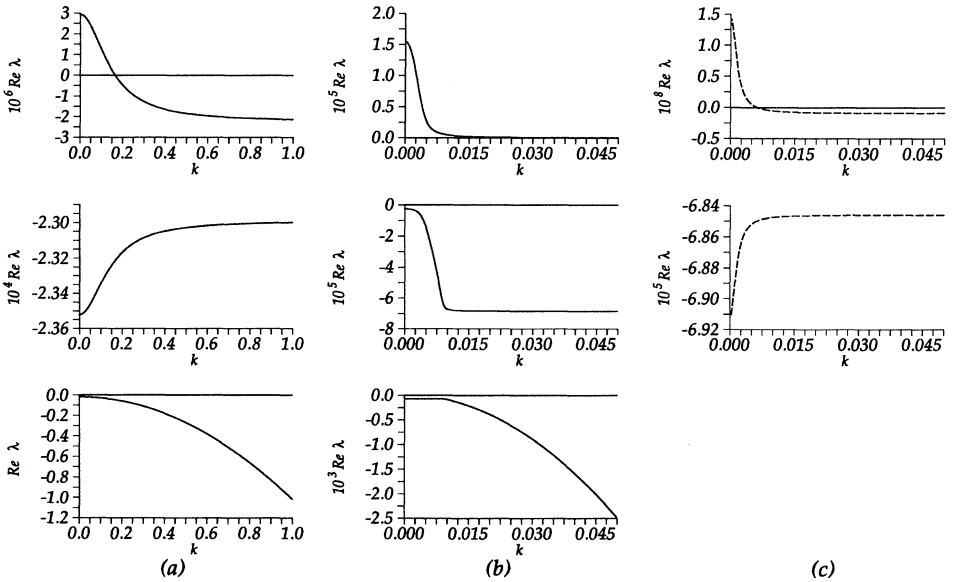

FIG. 2. The eigenmode spectrum (a) $j_0=0.001$ and (b) and (c): $j_0=2.3\times10^{-7}$. In (a), the full solution (continuous line) and the approximation (13) of a lifetime semiconductor (dashed) coincide, while in (b) and (c) they are significantly different for the upper two branches of the dispersion relation $\lambda(k)$. (λ in units of $1/\tau_M^*$, k in units of $1/L_D$.)

V. DYNAMICS OF INHOMOGENEOUS FILAMENTARY STATES

In order to obtain more insight into the nonlinear dynamic behavior of the system, we have analyzed (2)–(6) numerically. Depending on the actual ratio of the relevant time scales, different strategies have to be applied for this purpose. For higher current densities, where the dielectric relaxation is very fast compared to the GR processes, we can eliminate the electric field adiabatically. This implies for the longitudinal field

$$\mathcal{E}_x = \frac{j_0}{\mu \langle n \rangle} \ . \tag{25}$$

The transverse displacement current density can also be neglected, which implies that the drift current density $\mu n \mathcal{E}_z$ is compensated for by the diffusion current density $-\mu \partial n / \partial z$. Physically, this means that the transport of the free carriers due to drift and diffusion is much faster than GR processes. The carriers rearrange themselves instantaneously (on the faster time scale τ_M^*) in such a manner that

$$\frac{\partial n}{\partial z} = n \mathcal{E}_z \tag{26}$$

is satisfied. There remains a *local* dynamics,

$$\frac{\partial n}{\partial t} = \phi(n, \vec{n}_t, \mathcal{E}) \ , \tag{27}$$

together with (3) and the additional constraints (4), (25), and (26).

In the intermediate time-scale regime, the full dynamic system has to be taken into account.

For the simulation, we use the method of particles.[28,29] We divide the cross section of the sample into N equal cells. In each cell C_i $(i=1,\ldots,N)$ we assume homogeneously distributed carrier densities $n^{(i)}$ and $\vec{n}_t^{(i)}$, which are considered as "macroparticles." This allows us to write the charge density as

$$\rho(z,t) = \sum_{i=1}^{N} \rho^{(i)}(t) \Theta_i(z,t) \ , \tag{28}$$

with

$$\rho^{(i)}(t) = -1 + n^{(i)}(t) + \sum_{j=1}^{M} n_j^{(i)}(t) \ , \tag{29}$$

where

$$\Theta_i(z,t) = \begin{cases} 1 & \text{for } z \in [z^{(i)} - h/2, z^{(i)} + h/2] \\ 0 & \text{otherwise} \ . \end{cases} \tag{30}$$

$z^{(i)} = (i - 1/2) W/N$ is the center of the macroparticle i. We obtain the transverse electric field in the center of each cell $\mathcal{E}_z^{(i)}(t) = \mathcal{E}_z(z^{(i)}, t)$ by integration of (4):

$$\mathcal{E}_z^{(i)} = \mathcal{E}_z^{(0)} + h \left[\frac{\rho^{(i)}}{2} + \sum_{j=1}^{i-1} \rho^{(j)} \right] \ , \tag{31}$$

where $h = W/N$ is the length of each cell and $\mathcal{E}_z^{(0)}$ is the boundary condition $\mathcal{E}_z(0,t)$. The carrier densities $n^{(i)}$ can vary in the time interval Δt due to drift, diffusion, and GR processes. Δt is assumed to be so short that we can consider only the linearized processes.

The center $z^{(i)}$ of each macroparticle will move in Δt due to the drift according to

$$z^{(i)} \mapsto z^{(i)} + \mu \mathcal{E}_z^{(i)} \Delta t \ . \tag{32}$$

The weight of each macroparticle varies due to GR processes:

$$n^{(i)} \mapsto n^{(i)} + \phi(n^{(i)}, \vec{n}_t^{(i)}, \mathcal{E}_z^{(i)}) \Delta t \ . \tag{33}$$

The trapped carriers are treated in a similar manner.

The diffusion tends to expand a macroparticle, and decrease its weight by

$$h \mapsto h + \Delta h = h + \frac{2\mu \Delta t}{h} \ , \tag{34}$$

$$n^{(i)} \mapsto n^{(i)} \frac{h}{h + \Delta h} \ . \tag{35}$$

The latter is a good approximation if $\Delta h \ll h$, thus $\Delta t \ll h^2/(2\mu)$.

The above mappings are performed for all cells. The new carrier distribution is calculated via

$$n(z, t + \Delta t) = \sum_{i=1}^{N} n^{(i)}(t + \Delta t) \Theta_i(z, t + \Delta t) \ . \tag{36}$$

For the next time step, new macroparticles are created from the former ones with the initial center $z^{(i)} = (i - 1/2) W/N$ and cell length $h = W/N$, but a different weight, calculated through integration of (36):

$$n^{(i)} = \int_{z^{(i)} - h/2}^{z^{(i)} + h/2} n(z, t + \Delta t) dz \ . \tag{37}$$

From the "particles" point of view, appropriate boundary conditions are causing particle flow to vanish at each boundary. So if a macroparticle or a part of it attempts to cross the boundary of the sample, it is forced to remain in cell C_1 or C_N, respectively.

From a macroscopic point of view, appropriate boundary conditions are fixed values of the transverse electric field at the boundaries $\mathcal{E}_z(0,t) = \mathcal{E}_z(W,t) = 0$. The above-mentioned particle conservation implies global charge neutrality, i.e.,

$$Q = \int_0^W \rho(z,t) dz = 0 \ . \tag{38}$$

This together with (4) ensures $\mathcal{E}_z(0,t) = \mathcal{E}_z(W,t)$. Since these values can be controlled via the integration constant $\mathcal{E}_z^{(0)}$, the "macroscopic" boundary conditions are fulfilled.

For the intermediate time-scale regime, the above algorithm is implemented as described. Additionally, the dynamics of the longitudinal field has to be taken into account.

For the lifetime regime, the difference between the time scales of the GR and transport processes does not allow a direct application of the algorithm. As described above, the dynamics of the electric field can be eliminated adiabatically. The remaining local dynamics (27) and (3) can be solved fast with a second-order Runge-Kutta method.[30] In addition to the Poisson equation (4), Eq.

(26) has to be observed. This is done by a relaxation method with the aid of the above algorithm. The steady-state solution of the continuity equation

$$\frac{\partial n}{\partial t} = -\frac{\partial (n v_z)}{\partial z} \tag{39}$$

is found with the particle algorithm (the GR part being omitted). With the boundary condition $v_z(0)=v_z(W)=0$, this solution satisfies (26).

Following an analytical investigation,[8,9,19] we expect stable stationary filaments for the case of *lifetime* semiconductors for infinite boundary conditions. It was suggested[19] that if the dielectric relaxation of the electric field slows down, an oscillatory instability becomes possible. This idea leads to "breathing filaments," i.e., current filaments with fixed peak carrier density but oscillating walls. A model for the dynamics of the filament walls[13] shows a Hopf bifurcation leading to periodic oscillations of the filament walls and hence of the current at low current densities j_0, while at higher current densities the filaments are stable.

Our numerical simulations corroborate these approximate analytical results. For higher current densities, in the lifetime regime, we indeed find stable stationary filaments. Figure 3(a) shows a stable filament at the boundary of the sample. The time series of $\mathcal{E}_x$ and the transverse voltage $U_z=\int_0^W \mathcal{E}_z dz$ indicates a stable structure asymptotically approached after some transient oscillations. Lowering the current density, the filament walls become unstable, which leads to small self-sustained oscillations of the macroscopic variables $\mathcal{E}_x, \langle n \rangle, U_z$. These can be identified as "breathing" filaments. A further reduction of the current density results in a new spatiotemporal instability: the above-described breathing motion grows in time until the filament is detached from the boundary $z=W$ and travels to the other side ($z=0$), where a similar breathing instability develops. As a result, the whole filament travels intermittently from one side of the sample to the other, and vice versa. The spatially averaged carrier density and the field $\mathcal{E}_x$ show chaotic bursts with very low frequencies as compared to the former regular breathing oscillations. During the laminar periods between the bursts, the filament is pinned to either of the boundaries, which is indicated by approximately constant positive or negative transverse voltage U_z, respectively.

The different possible spatiotemporal dynamic states of the filament, which occur successively with decreasing current density, are shown in Fig. 4 for a wider sample: in Fig. 4(a), a stable filament is built up after transient oscillations; Fig. 4(b) shows a breathing filament, whose position is displaced erratically (intermittently); in Fig. 4(c), a filament arises and splits temporarily into two. Eventually, in Fig. 4(d), one of these vanishes due to a competition process between these two filaments analogous to Ostwald ripening.[31,32] The motion of the remaining filament is accompanied by a change in its form and position.

While the stationary filament is symmetric, the traveling filament is asymmetric. Figure 5 shows the carrier density of a traveling filament (obtained with cyclic boundary conditions in order to avoid pinning at the boundaries). Its leading edge is steeper than its trailing edge. According to (6), $\mathcal{E}_z$ tends to change in time until

$$\mathcal{E}_z = \frac{\partial \ln n}{\partial z} \tag{40}$$

holds. Thus the electric field is large at the leading edge of the filament and small at its trailing edge. The higher electric field at the front end leads to a higher impact ion-

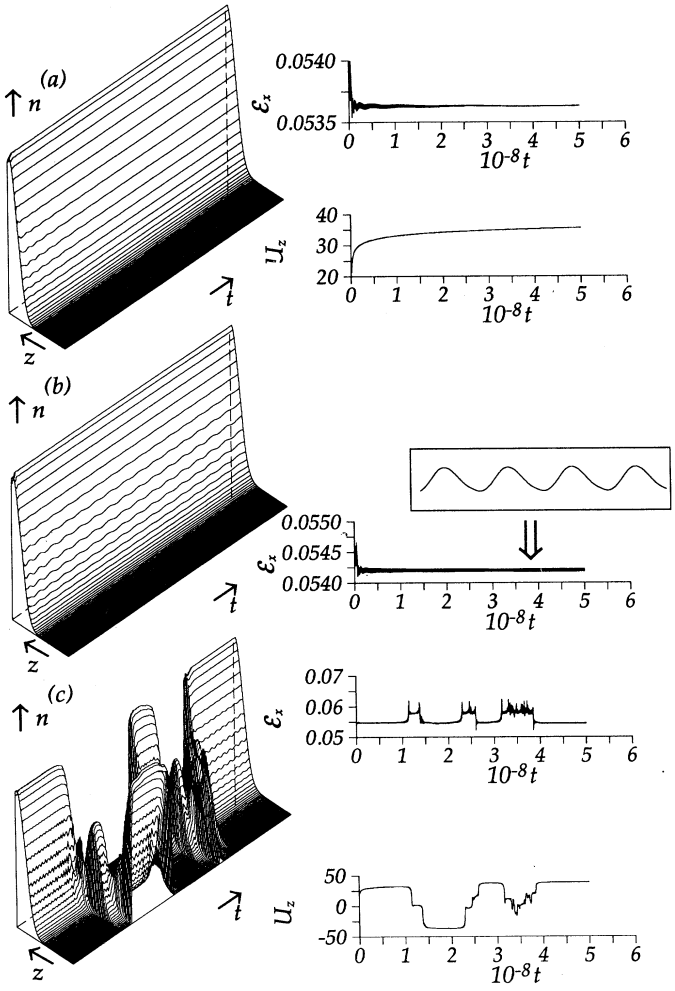

FIG. 3. The carrier density n as a function of the lateral coordinate z and time t for (a) $j_0=0.000\,22$. The maximum n is $0.0246N_A^*$. The associated time series of the longitudinal electric field $\mathcal{E}_x$ and the transverse voltage U_z indicates a stable filament after a few transient oscillations. (b) Small periodic breathing oscillations for $j_0=0.000\,205$. The maximum n is $0.0227N_A^*$. The inset shows the self-sustained oscillations of $\mathcal{E}_x$ in an enlarged scale: The duration of the signal in the inset is $1.75\times10^6\tau_M^*$, the amplitude is $2\times10^{-5}\mathcal{E}_0$. (c) Intermittent traveling filament for $j_0=0.0002$. The maximum n is $0.0275N_A^*$. The simulated time interval is $T=5\times10^8\tau_M^*=0.5$ ms, the width of the sample is $W=1000L_D=56$ μm. The units of $\mathcal{E}_x$ and U_z are $\mathcal{E}_0=60.8$ V/cm and $\mathcal{E}_0L_D=0.34$ mV, respectively.

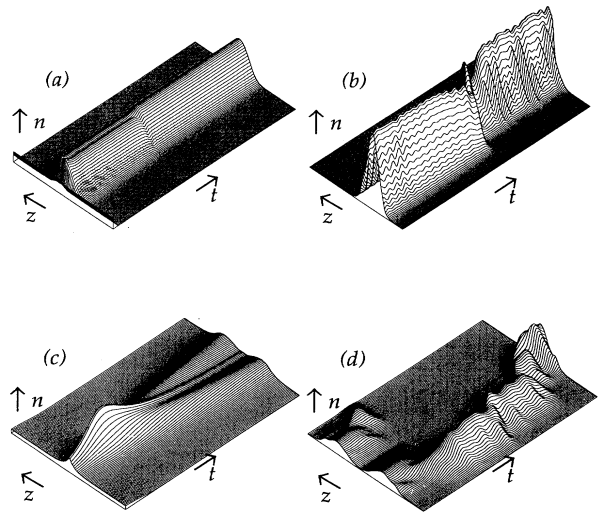

FIG. 4. Different types of spatiotemporal dynamics: (a) $j_0=0.000\,45$ (simulated time interval $T=1.24\times10^8\tau_M^*$); (b) $j_0=0.0001$ ($T=1.6\times10^7\tau_M^*$); (c) $j_0=0.000\,05$ ($T=6\times10^6\tau_M^*$); and (d) the same as (c) but for the simulated time interval from $t=1\times10^7\tau_M^*$ to $t=2.3\times10^7\tau_M^*$. The width of the sample is $W=2000L_D$.

ization rate and thus to an increase of the carrier density. At the back end, the carrier concentration decreases due to the lower electric field. As a result, both walls of the filament move in the same direction, i.e., the filament travels to one side. This asymmetry of the concentration profile of traveling current filaments is inverse to the asymmetry of the field profile in the case of traveling field domains, e.g., in the Gunn effect.[33]

The motion of the filament through the sample may be suppressed by inhomogeneities such as roughness in the contact region, or inhomogeneous doping. We have investigated the situation for a slightly higher doping in the center of the sample. For current densities larger than a minimum value, this inhomogeneity is able to *pin* the filament.[34] While the position of the filament is fixed at the inhomogeneity, the walls still show breathing oscillations [Fig. 6(a)]. Intermittent destruction and renascence of the filament is also possible [Fig. 6(b)]. For smaller current densities the dielectric relaxation time becomes so long that the dielectric relaxation is no longer strong enough to force pinning against the random transverse motion of the filaments. Experiments to check these theoretical predictions would be desirable.

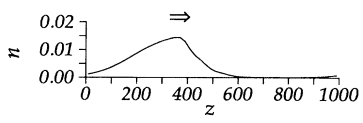

FIG. 5. The carrier density n as a function of z at a fixed time for $j_0=0.0002$ with cyclic boundary conditions. The arrow indicates the direction of the traveling filament. The width is $W=1000L_D$.

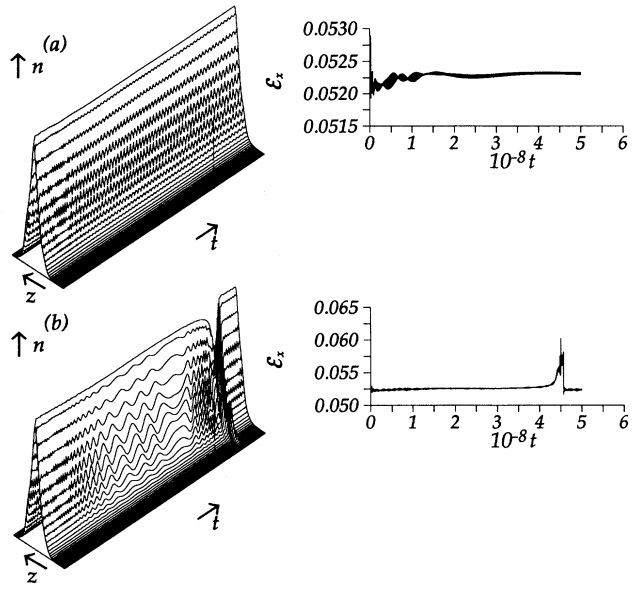

FIG. 6. Dynamics of the carrier density $n(z,t)$ in a modulation-doped sample with width of $W=1000L_D$ and the corresponding time series of the longitudinal field $\mathcal{E}_x$ for (a) $j_0=0.000\,21$ and (b) $j_0=0.000\,22$. The acceptor concentration is 15% higher than in the rest of the sample within a layer of $120L_D$ in the center of the sample.

VI. CONCLUSIONS

We have presented a macroscopic model for the spatiotemporal nonlinear dynamics of current transport in semiconductors at low temperatures, based on a microscopic transport description of the scattering and generation-recombination processes, in particular impact ionization of impurities by Monte Carlo simulations. Our numerical simulation method allows for the treatment of the different time scales involved. The model shows a bifurcation scenario (with decreasing current) from homogeneous states to stable filaments, breathing filaments, and traveling filaments, including novel complex spatiotemporal intermittent behavior in which a breathing instability triggers spatiotemporal intermittency of filaments traveling from one side of the sample to the other. We suggest that this complex oscillatory instability offers the first detailed explanation of the chaotic spatiotemporal oscillations observed in p-Ge at 4 K.[35]

The physical origin of the oscillatory instability is based upon the autocatalytic impact ionization process of the acceptor ground and first excited states. A fluctuation of the carrier concentration in the filament wall tends to increase due to impact ionization. In the lifetime regime, this excess carrier density can be distributed effectively via drift and diffusion processes leading to stable filaments. For smaller current densities, the transverse electric field reacts too slowly upon such fluctuations, which allow the fluctuations to increase further and trigger instabilities.

We would like to point out the different time scales of the breathing filament oscillations and the traveling fila-

ment oscillations. These time scales are connected with different dielectric relaxation times: the breathing filament oscillation mode is localized at the filament wall, where the carrier density is orders of magnitude higher than outside the filament, leading to a short dielectric relaxation time and high-frequency oscillations. Outside the filament there are almost no free carriers, which results in very large GR and dielectric relaxation times. These very slow processes are responsible for the observed low frequencies. This solves the discrepancy existing hitherto between the frequencies obtained in experiments[4] and theories.[10,13]

ACKNOWLEDGMENTS

This work was partially supported by Alexander von Humboldt-Stiftung and Deutsche Forschungsgemeinschaft.

*On leave of absence from Institute of Semiconductor Physics, 2600 Vilnius, Lithuania.

[1]K. Aoki and K. Yamamoto, Phys. Lett. A **98**, 72 (1983).

[2]K. M. Mayer, J. Parisi, and R. P. Huebener, Z. Phys. B **71**, 171 (1988).

[3]J. Spangler, A. Brandl, and W. Prettl, Appl. Phys. A **48**, 143 (1989).

[4]K. M. Mayer, R. Gross, J. Parisi, J. Peinke, and R. P. Huebener, Solid State Commun. **63**, 55 (1987).

[5]R. Symanczyk, S. Gaelings, and D. Jäger, Phys. Lett. A **160**, 397 (1991).

[6]F.-J. Niedernostheide, M. Arps, R. Dohmen, H. Willebrand, and H.-G. Purwins, Phys. Status Solidi B **172**, 249 (1992).

[7]F.-J. Niedernostheide, B. S. Kerner, and H.-G. Purwins, Phys. Rev. B **46**, 7559 (1992).

[8]E. Schöll, Z. Phys. B **48**, 153 (1982).

[9]E. Schöll, Z. Phys. B **52**, 321 (1983).

[10]E. Schöll, Phys. Rev. B **34**, 1395 (1986).

[11]G. Hüpper, E. Schöll, and L. Reggiani, Solid-State Electron. **32**, 1787 (1989).

[12]G. Hüpper and E. Schöll, Phys. Rev. Lett. **66**, 2463 (1991).

[13]E. Schöll and D. Drasdo, Z. Phys. B **81**, 183 (1990).

[14]A. Brandl and W. Prettl, Phys. Rev. Lett. **66**, 3044 (1991).

[15]E. Schöll, in *Handbook on Semiconductors,* 2nd ed., edited by P. T. Landsberg (North-Holland, Amsterdam, 1992), Vol. 1, Chap. 8, pp. 419–447.

[16]J. Peinke, J. Parisi, A. Mühlbach, and R. P. Huebener, Z. Naturforsch. **42a**, 441 (1987).

[17]J. Peinke, J. Parisi, B. Röhricht, K. M. Mayer, U. Rau, and R. P. Huebener, Solid-State Electron. **31**, 817 (1988).

[18]W. Clauss, U. Rau, J. Peinke, J. Parisi, A. Kittel, M. Bayerbach, and R. P. Huebener, J. Appl. Phys. **70**, 232 (1991).

[19]E. Schöll, *Nonequilibrium Phase Transitions in Semiconductors* (Springer-Verlag, Berlin, 1987).

[20]G. Baccarani, M. Rudan, R. Guerrieri, and P. Ciampolini, Adv. CAD VLSI **1**, 107 (1986).

[21]E. Schöll, Solid-State Electron. **32**, 1129 (1989).

[22]G. Hüpper, E. Schöll, and A. Rein, Mod. Phys. Lett. B **6**, 1001 (1992).

[23]G. Hüpper, W. Quade, E. Schöll, and T. Kuhn (unpublished).

[24]M. Lax, Phys. Rev. **119**, 1502 (1960).

[25]V. N. Abakumov, V. I. Perel, and I. N. Yassievich, Fiz. Tekh. Poluprovodn. **12**, 3 (1978) [Sov. Phys. Semicond. **12**, 1 (1978)].

[26]L. Reggiani and V. V. Mitin, Rev. Nuovo Cimento **12** (1), 1 (1989).

[27]N. G. van Kampen, Phys. Rep. **124**, 70 (1985).

[28]A. Čenys, G. Lasiene, and K. Pyragas, Solid-State Electron. **35**, 975 (1992).

[29]R. W. Hockney and J. W. Eastwood, *Computer Simulation Using Particles* (McGraw-Hill, New York, 1981).

[30]W. H. Press, B. P. Flannery, S. A. Teukolsky, and W. T. Vettering, *Numerical Recipes* (Cambridge University Press, Cambridge, England, 1989).

[31]L. Schimansky-Geier, Ch. Zülicke, and E. Schöll, Z. Phys. B **84**, 433 (1991).

[32]R. E. Kunz and E. Schöll, Z. Phys. B **89**, 289 (1992).

[33]M. P. Shaw, V. V. Mitin, E. Schöll, and H. L. Grubin, *The Physics of Instabilities in Solid State Electron Devices* (Plenum, New York, 1992).

[34]B. S. Kerner and V. V. Osipov, Usp. Phys. Nauk **157**, 201 (1989) [Sov. Phys. Usp. **32**, 101 (1989)].

[35]U. Rau, W. Clauss, A. Kittel, M. Lehr, M. Bayerbach, J. Parisi, J. Peinke, and R. P. Huebener, Phys. Rev. B **43**, 2255 (1991).